Article

Cell Reports

PCNA Unloading Is Negatively Regulated by BET Proteins

Graphical Abstract

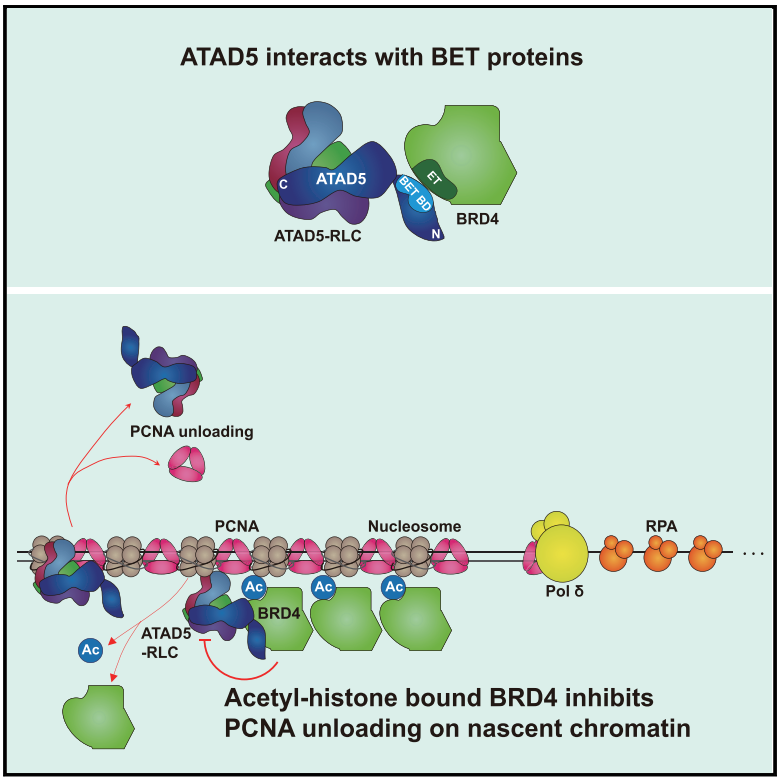

Authors

Mi-Sun Kang, Jinwoo Kim, Eunjin Ryu, ..., Jung Me Hwang, Kyungjae Myung, Sukhyun Kang

Correspondence

kmyung@ibs.re.kr (K.M.),
kangsh@ibs.re.kr (S.K.)

In Brief

Kang et al. demonstrate how PCNA unloading is regulated on nascent chromatin. Timely PCNA unloading from replicated DNA is crucial for faithful DNA replication. BRD4 binds to ATAD5, a subunit of PCNA-unloading complex. Acetyl-histone-bound BRD4 inhibits the activity of ATAD5 complex on nascent chromatin to prevent premature PCNA unloading.

Highlights

- ATAD5 and BRD4 are enriched on nascent DNA
- A conserved region upstream of ATAD5 PCNA-unloading domain binds to BRD4 ET domain
- Acetyl-histone-bound BRD4 inhibits PCNA unloading by ATAD5-RLC on nascent DNA

Kang et al., 2019, Cell Reports *29*, 4632–4645
December 24, 2019
https://doi.org/10.1016/j.celrep.2019.11.114

CellPress

OPEN ACCESS
CellPress

Cell Reports
Article

PCNA Unloading Is Negatively Regulated by BET Proteins

Mi-Sun Kang,[1] Jinwoo Kim,[1,2] Eunjin Ryu,[1,2] Na Young Ha,[1] Sunyoung Hwang,[1] Byung-Gyu Kim,[1] Jae Sun Ra,[1] Yeong Jae Kim,[1,2] Jung Me Hwang,[1] Kyungjae Myung,[1,2,*] and Sukhyun Kang[1,3,*]

[1]Center for Genomic Integrity, Institute for Basic Science, Ulsan 44919, Republic of Korea
[2]School of Life Sciences, Ulsan National Institute of Science and Technology, Ulsan 44919, Republic of Korea
[3]Lead Contact
*Correspondence: kmyung@ibs.re.kr (K.M.), kangsh@ibs.re.kr (S.K.)
https://doi.org/10.1016/j.celrep.2019.11.114

SUMMARY

Proliferating cell nuclear antigen (PCNA) is a DNA clamp essential for DNA replication. During DNA synthesis, PCNA is continuously loaded onto and unloaded from DNA. PCNA recruits various proteins to nascent DNA to facilitate chromosome duplication. Therefore, timely PCNA unloading is crucial for high-fidelity DNA replication. The ATAD5-RFC-like complex (ATAD5-RLC) unloads PCNA from replicated DNA. It is unclear how ATAD5-RLC activity is regulated to prevent premature PCNA unloading. Here, we find that BRD4, an acetyl-histone-binding chromatin reader, inhibits the PCNA-unloading activity of ATAD5-RLC. The BRD4 ET domain interacts with a region upstream of the ATAD5 PCNA-unloading domain. BRD4-ATAD5 binds to acetyl-histones in nascent chromatin. BRD4 release from chromatin correlates with PCNA unloading. Disruption of the interaction between BRD4 and acetyl-histones or between BRD4 and ATAD5 reduces the PCNA amount on chromatin. In contrast, the overexpression of BRD4 increases the amount of chromatin-bound PCNA. Thus, acetyl-histone-bound BRD4 fine-tunes PCNA unloading from nascent DNA.

INTRODUCTION

Eukaryotic DNA replication is tightly regulated for the accurate duplication of the genome (Kang et al., 2018). During DNA replication, many kinds of replication proteins sequentially associate with replication forks. Timely assembly and disassembly of replication machinery on replicating DNA are crucial for efficient and accurate DNA replication.

Proliferating cell nuclear antigen (PCNA) is a DNA clamp that tethers DNA polymerases to replicating DNA to enhance polymerase processivity. PCNA functions as a molecular platform for many proteins that participate in DNA replication and repair (Moldovan et al., 2007). PCNA also plays important roles in nascent chromatin assembly. PCNA interacts with CAF-1, a histone chaperone, and participates in nucleosome deposition on nascent DNA (Shibahara and Stillman, 1999; Zhang et al., 2000). An interplay between PCNA and the BAZ1B-SMARCA5 complex, a chromatin remodeler, was also reported (Poot et al., 2004). The BAZ1B-SMARCA5 complex and PCNA work together to appropriately assemble nascent chromatin.

PCNA must be removed from DNA after DNA synthesis and nascent chromatin assembly. The prolonged presence of PCNA on replicated chromatin results in the inappropriate recruitment of replication proteins that causes genome instability (Lee et al., 2013). PCNA is a homotrimer that forms a closed ring. The PCNA ring needs to be opened and closed to encircle DNA. DNA loading and unloading of PCNA are mediated by three clamp-loader complexes: replication factor C (RFC) and two RFC-like complexes (RLCs). RFC and CTF18-RLC load PCNA onto primer-template junctions, and ATAD5-RLC unloads PCNA (Kang et al., 2018, 2019). PCNA unloading by ATAD5-RLC is important for the maintenance of genomic integrity (Lee et al., 2013).

DNA replication is tightly coupled with chromatin disassembly and reassembly (Kurat et al., 2017; Petryk et al., 2018; Reveron-Gomez et al., 2018; Yu et al., 2018). Parental nucleosomes are dismantled ahead of replicative helicase. Behind the replication fork, nucleosomes are reassembled on DNA immediately after DNA synthesis. During nascent chromatin assembly, disassembled parental histones are transferred to newly replicated DNA. Along with parental histones, newly synthesized histones are deposited on nascent DNA. In a human cell, new histones are acetylated at K5 and K12 of histone H4 (Loyola et al., 2006; Sobel et al., 1995).

Histone modifications, such as acetylation and methylation, are recognized by chromatin readers. Each chromatin reader binds to distinctively modified histones and recruits effector molecules to the chromatin. BET family proteins, such as BRD2, BRD3, and BRD4, are chromatin readers that specifically bind to acetylated histones. Two bromodomains (BDs) in BET proteins recognize acetylated histones. BET proteins have an additional conserved domain called the extra-terminal (ET) domain. Through the ET domain, BET proteins interact with a wide range of effector molecules that regulate transcription, DNA replication, and repair (Donati et al., 2018).

Because BRD4 is a key transcription regulator for many essential genes, the biological functions of BRD4 have been

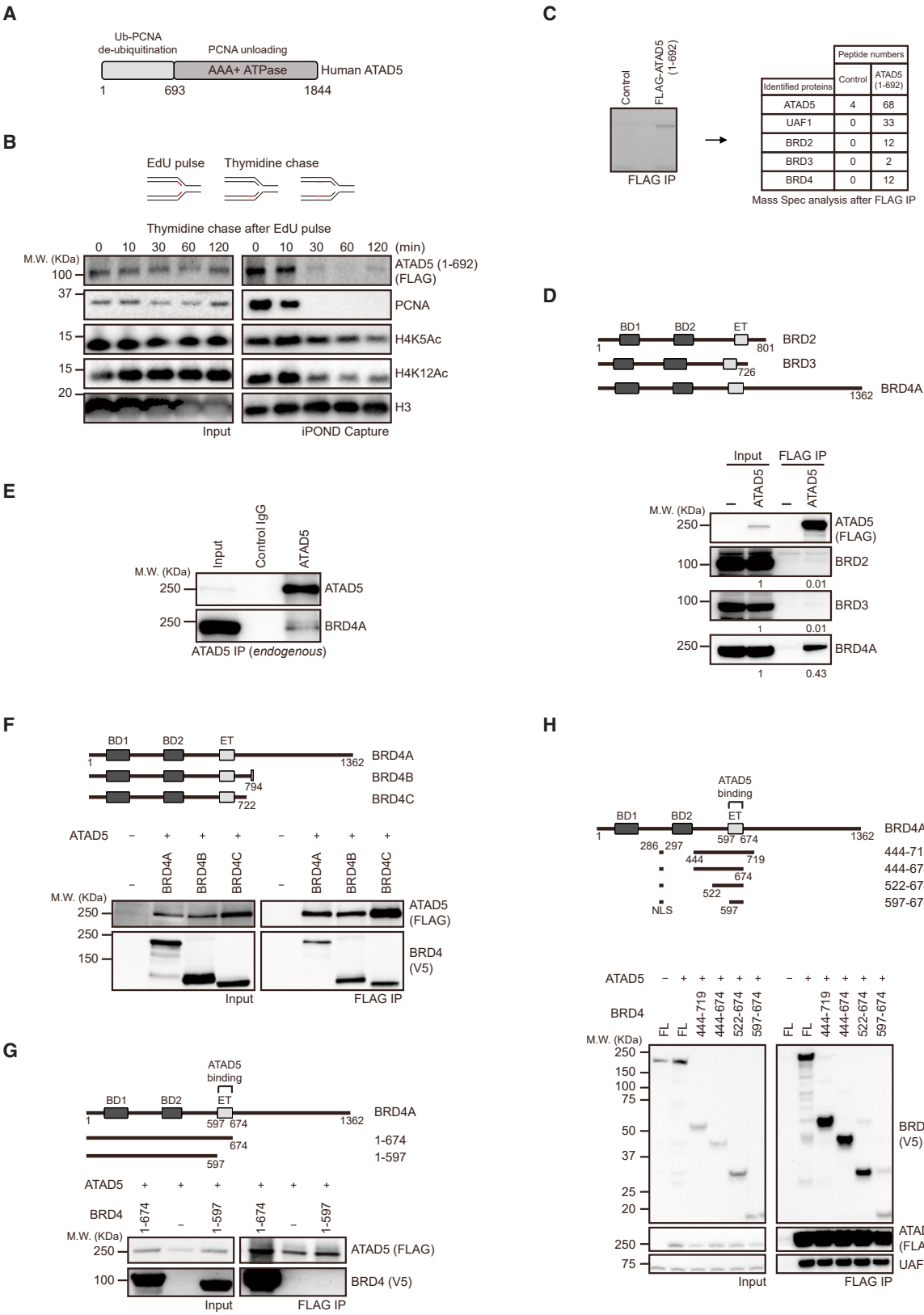

(legend on next page)

investigated thoroughly. BRD4 recruits different kinds of transcriptional regulators to acetylated chromatin and organizes super-enhancers (Sabari et al., 2018). BRD4 interacts with histone modifiers such as JMJD6 and NSD3 and chromatin remodelers such as CHD4 to facilitate transcription initiation (Jones and Lin, 2017; Konuma et al., 2017; Liu et al., 2013; Shen et al., 2015; Zhang et al., 2016). BRD4 also binds to the positive transcription elongation factor b (P-TEFb) and promotes transcription elongation (Jang et al., 2005; Yang et al., 2005). Growing evidence suggests that BRD4 performs important functions in DNA replication and repair. BRD4 recruits TICRR to euchromatin for timely replication initiation (Sansam et al., 2018). TICRR is a helicase-activating protein that is required for replication origin firing. BRD4 binds to RFC, and their interaction is reported to be important for proper S phase progression (Maruyama et al., 2002). During double-strand break repair, BRD4 interacts with 53BP1 and stabilizes it at the break sites (Li et al., 2018). BRD4 is regarded as a major therapeutic target in many diseases because of its pivotal roles in cell proliferation (Korb et al., 2017; Sun et al., 2018; White et al., 2019).

Given that PCNA is important for nascent chromatin assembly, PCNA unloading from nascent DNA should be coordinated with nucleosome deposition. In yeast, Elg1, a homolog of ATAD5, cooperates with histone chaperone Rtt106 to facilitate nascent chromatin organization (Gali et al., 2018). Nevertheless, researchers have not fully elucidated how the activity of ATAD5-RLC is regulated to coordinate PCNA unloading with nascent chromatin assembly.

Here, we found that BET proteins fine-tune the PCNA-unloading activity of ATAD5-RLC. The ET domain of BRD4 interacted with an ATAD5 fragment (positions 596–692, hereafter called ATAD5 (596–692)) that is located immediately upstream of the PCNA-unloading domain. Acetyl-histone-bound BRD4 inhibited the PCNA-unloading activity of ATAD5-RLC. Our results suggest that PCNA unloading from replicated DNA is regulated by the acetylation status of nascent chromatin.

RESULTS

ATAD5 Is Enriched on Nascent DNA

Human ATAD5 is a multi-domain protein (Figure 1A) (Kang et al., 2019). ATAD5 (693–1,844) interacts with RFC2-5 to form an RLC that has a PCNA-unloading activity. The N-terminal domain of ATAD5 interacts with UAF1 and participates in the deubiquitination of ubiquitinated PCNA (Lee et al., 2010). As expected from its replication-related functions, iPOND (isolation of proteins on nascent DNA) analysis showed that ATAD5 was enriched on nascent DNA (Figure S1A) (Lopez-Contreras et al., 2013). ATAD5 dissociated from nascent DNA after a thymidine chase procedure, when PCNA disappeared from the nascent DNA. Of note, ATAD5 (1–692) was more strongly enriched on nascent DNA as compared to ATAD5 (693–1,844) (Figures 1B and S1B). The release time of ATAD5 (1–692) from nascent DNA was similar to that of PCNA. Because ATAD5-RLC functions as a PCNA unloader, the coexistence of PCNA and ATAD5 (1–692) on nascent DNA implies that the unloading activity of ATAD5-RLC may be regulated through its N-terminal domain.

The ET Domain of BET Proteins Interacts with ATAD5

In addition to the UAF1-binding motif, ATAD5 (1–692) contains several well-conserved motifs whose functions have not been characterized (Figure S1C). These motifs may act as docking interfaces for a regulatory factor that controls ATAD5-RLC activity. To uncover the functional regulators of ATAD5-RLC, we affinity purified ATAD5 (1–692) after transient expression. Mass spectrometric analysis was performed for the identification of the coisolated proteins (Figure 1C). Enrichment of UAF1 with ATAD5 (1–692) validated our experimental setup (Lee et al., 2010). Moreover, BET proteins—BRD2, BRD3, and BRD4—were found to be coisolated with ATAD5 (1–692). BET proteins are known to interact with acetyl-histones such as H4K5Ac and H4K12Ac, which are enriched in nascent chromatin (Figures 1B and S1A). Our iPOND analysis showed that BRD4 was recruited to the nascent

Figure 1. BET Proteins Interact with the N-Terminal Domain of ATAD5

(A) The domain diagram of human ATAD5. The N-terminal domain of ATAD5 interacts with UAF1 and participates in deubiquitination of ubiquitinated PCNA. The C-terminal AAA^+ ATPase domain of ATAD5 and RFC2–5 form an RFC-like complex (RLC) that possesses PCNA-unloading activity.

(B) ATAD5 (1–692) binds to nascent DNA. iPOND analysis was performed after the EdU pulse-chase procedure. Cells transiently expressing ATAD5 (1–692) were harvested at indicated time points after the thymidine chase. Endogenous ATAD5 was depleted by siRNA. The association of the indicated proteins with nascent DNA was analyzed by immunoblotting.

(C) BET proteins bind to ATAD5 (1–692). Affinity purification mass spectrometry (AP-MS) was performed with FLAG-ATAD5 (1–692). Left panel: FLAG-immunoprecipitated proteins were analyzed by SDS-PAGE with Coomassie staining. Right panel: BRD2, BRD3, and BRD4 were enriched in the FLAG immunoprecipitate of FLAG-ATAD5 (1–692). MS results are summarized and highly enriched proteins are shown in the table.

(D) ATAD5 interacts with BRD2, BRD3, and BRD4. Transiently expressed full-length FLAG-ATAD5 was immunoprecipitated, and coprecipitations of endogenous BRD2, BRD3, and BRD4 were analyzed by immunoblotting. BRD4 was more enriched in the immunoprecipitate as compared to BRD2 or BRD3. Numbers below each blot indicate the relative amount of BRD2, BRD3, or BRD4.

(E) Endogenous ATAD5 interacts with BRD4A. Endogenous ATAD5 was immunoprecipitated using an anti-ATAD5 antibody, and coisolation of endogenous BRD4A was analyzed by immunoblotting.

(F) ATAD5 interacts with all three isoforms of BRD4. Top panel: a domain diagram of BRD4 isoforms. Bottom panel: FLAG-immunoprecipitation was performed on the lysates of cells transiently coexpressing FLAG-ATAD5 and V5-tagged BRD4 isoforms.

(G) The BRD4 ET domain is crucial for ATAD5 binding. Top panel: a diagram of BRD4 mutants examined for ATAD5 interaction. Numbers indicate positions of deletion. Bottom panel: the interactions between FLAG-ATAD5 and V5-tagged BRD4 mutants were analyzed by FLAG-immunoprecipitation. The ET domain-null BRD4 mutant failed to interact with ATAD5.

(H) The BRD4 ET domain is an ATAD5-interacting motif. Top panel: a diagram of BRD4 mutants examined for ATAD5 interaction. Numbers indicate positions of deletion. The nuclear localization signal (NLS) of BRD4, BRD4 (286–297), was fused to N-terminal deletion mutants of BRD4. The ET domain of BRD4, BRD4 (597–674), was sufficient for ATAD5 binding.

See also Figure S1.

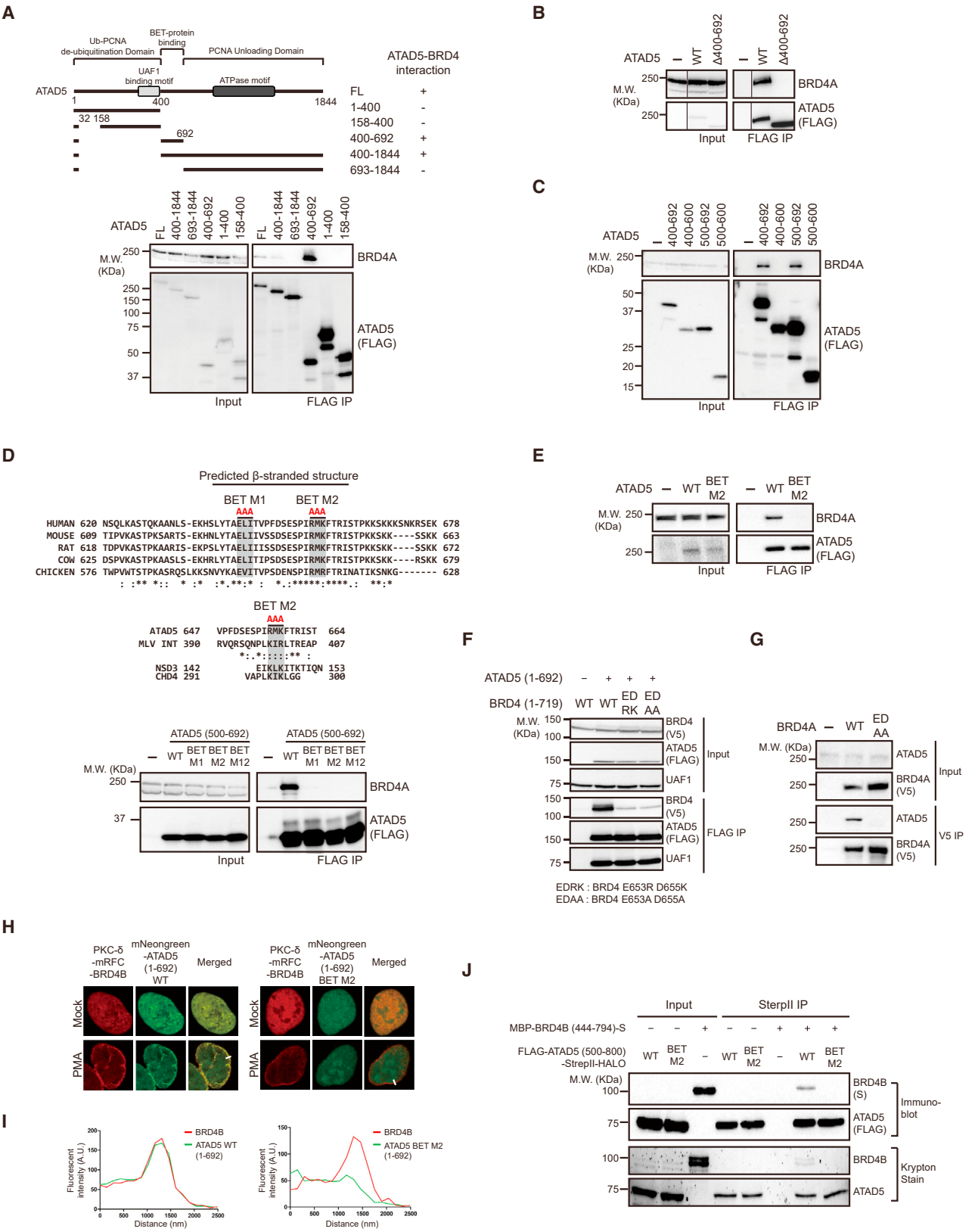

(legend on next page)

chromatin where acetyl-histones were enriched (Figure S1A). BRD4 dissociated from nascent DNA after the thymidine chase procedure. Given that reduction in the amount of acetyl-histones coincides with the dissociation of BRD4 and PCNA from nascent DNA, BET proteins may regulate PCNA unloading from nascent DNA. To understand how BET proteins control the activity of ATAD5-RLC, we first investigated the interaction between them (Figure 1D). In agreement with affinity purification mass spectrometry (AP-MS) results (Figure 1C), endogenous BRD2, BRD3, and BRD4 were coprecipitated with FLAG-ATAD5. BRD4 was more enriched with ATAD5 as compared to BRD2 and BRD3. This result suggests that BRD4 could be a major regulator of ATAD5-RLC. The immunoprecipitation of endogenous ATAD5 confirmed the binding of ATAD5 to BRD4 (Figure 1E). In human cells, BRD4 is expressed as three isoforms, BRD4A, BRD4B, and BRD4C (Figure 1F). All three isoforms contain BD1 and BD2 and an ET domain. BRD4A contains a long C-terminal domain that is crucial for its function as a transcriptional regulator. BRD4B lacks the C-terminal domain of BRD4A but contains a unique 78-amino acid sequence at its C terminus. BRD4B is known to regulate chromatin compaction (Floyd et al., 2013). BRD4C is the shortest isoform. We examined the interactions between V5-tagged BRD4 isoforms and FLAG-ATAD5 after transient coexpression (Figure 1F). All three BRD4 isoforms robustly bound to ATAD5. Because BRD4A is the most abundant isoform in human cells (Figure S1D), BRD4A may be a major interacting partner of ATAD5 among BET proteins.

To identify the ATAD5-binding motif in BRD4, we prepared a series of BRD4 deletion mutants and examined their interactions with ATAD5 (Figures 1G and 1H). Immunoprecipitation with C-terminal deletion mutants of BRD4 revealed that the BRD4 ET domain was crucial for ATAD5 binding (Figure 1G). An ET domain-null BRD4 fragment, BRD4 (1–597), failed to interact with ATAD5. Next, we tested whether the region upstream of the BRD4 ET domain is essential for ATAD5 binding (Figure 1H). Given that BRD4 (286–297) functions as a nuclear localization signal (NLS), we fused this NLS sequence to the N-terminal-deletion mutants of BRD4. Immunoprecipitation results showed that the ET domain alone could bind to ATAD5. These results suggested that BRD4 interacts with ATAD5 through its ET domain. ATAD5 showed different binding affinities for different BET proteins (Figure 1D), although the sequences of ET domains are very similar among BRD2, BRD3, and BRD4 (Figure S1E). Regions upstream of the ET domain may have enhanced the interaction between BRD4 and ATAD5 (Figure 1H). BRD4 fragments that contain a region upstream of the ET domain more robustly bound to ATAD5 as compared to the ET domain alone.

Next, we determined whether DNA damage signaling affects the BRD4-ATAD5 interaction (Figure S1F). ATAD5 was immunoprecipitated from cells to which 50 J/m^2 UV (harvested after 6 h), 2 mM hydroxyurea (6 h), or 0.02% of methyl methane sulfonate (MMS, 2 h) was applied. Amounts of coprecipitated BRD4 were not significantly different among the treatments with the DNA-damaging agents. Therefore, the BRD4-ATAD5 interaction was not regulated by the DNA damage response.

ATAD5 (596–692) is an ET Domain-Binding Motif

Mutations in the BRD4 ET domain could affect various cellular processes because BRD4 interacts with several key regulatory proteins through its ET domain. Therefore, we tried to identify ATAD5 mutations that specifically disrupt the binding to BRD4 to understand the biological function of the BRD4-ATAD5 interaction. We prepared several deletion mutants of ATAD5 and examined their interaction with endogenous BRD4A (Figure 2A). ATAD5 (400–692) robustly bound to BRD4A, but ATAD5 (1–400) did not. This finding was supported by AP-MS data (Figure S2A). The BRD4A polypeptide (250 kDa) was robustly enriched with FLAG-ATAD5 (400–692). An ATAD5 fragment that lacks a polypeptide between the 400th and the 692nd amino acid residues

Figure 2. ATAD5 Interacts with BRD4 through a Conserved BET Protein-Binding Domain

(A) ATAD5 (400–692) binds to BRD4. Top panel: ATAD5 mutants examined for BRD4 binding. Numbers indicate the positions of deletion. The NLS of ATAD5, ATAD5 (1–32), was fused to the N-terminal-deletion mutants of ATAD5. Bottom panel: the interaction between endogenous BRD4A and FLAG-ATAD5 fragments was examined by FLAG-immunoprecipitation.

(B) ATAD5 (400–692) is crucial for BRD4 binding. Interactions between endogenous BRD4A and FLAG-ATAD5 (Δ400-692) were examined by FLAG-immunoprecipitation.

(C) ATAD5 (600–692) is a BET protein-binding domain, BET BD. Interactions between endogenous BRD4A and the indicated FLAG-ATAD5 fragments were analyzed by immunoblotting.

(D) Conserved residues in the BET BD are essential for ATAD5 interaction. Mutations in the predicted β-stranded structure of BET BD abrogated the BRD4-ATAD5 interaction. Top panel: the ATAD5 BET BD is well conserved among species. Positions of BET M1 ($E^{643}LI^{645}$ to AAA) and BET M2 ($R^{656}MK^{658}$ to AAA) are indicated above the sequence alignment. Center panel: sequences around $R^{656}MK^{658}$ of ATAD5 are similar to the BRD4-binding motif of NSD3, CHD4, and of the MLV integrase. Bottom panel: binding of endogenous BRD4A to wild-type or mutant FLAG-ATAD5 (500–692) was analyzed. Mutations BET M1 and BET M2 abrogated the BRD4-ATAD5 interaction.

(E) Full-length FLAG-ATAD5 (BET M2) failed to interact with endogenous BRD4A.

(F) E^{653} and D^{655} of the BRD4 ET domain are crucial for the interaction with ATAD5. Binding of ATAD5 (1–692)-FLAG-mNeongreen to wild-type or mutant BRD4 (1–719) was analyzed by FLAG-immunoprecipitation. BRD4 (E653R, D655K) and BRD4 (E653A, D655A) failed to interact with ATAD5. ATAD5 binding to UAF1 was not affected by those mutations.

(G) Full-length BRD4A (E653A, D655A) failed to interact with endogenous ATAD5.

(H) CUPID analysis was performed to examine the interaction between BRD4B and ATAD5 (1–692). PKC-δ-mRFC-BRD4B and mNeongreen-ATAD5 (1–692) were cotransfected into 293T cells. After PMA treatment, nuclear membrane localization of each protein was analyzed by confocal microscopy. Wild-type ATAD5 (1–692) comigrated with BRD4B to the nuclear membrane, but the BET M2 mutant did not. White bars indicate the cross-section used for quantification.

(I) Quantification of data in (H).

(J) BRD4 directly interacts with ATAD5. Purified MBP-BRD4B (444–794)-S was mixed with either wild-type or BET M2 FLAG-ATAD5 (500–800)-StrepII-HALO. StrepII affinity purification was performed, and the isolated proteins were analyzed by either immunoblotting or Krypton staining. BRD4B (444–794) was found to be copurified with wild-type ATAD5 (500–800). Mutation BET M2 in ATAD5 abrogated the copurification.

See also Figure S2.

A

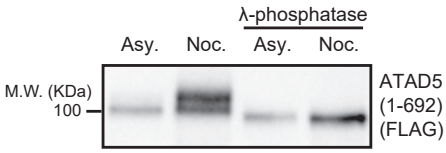

B

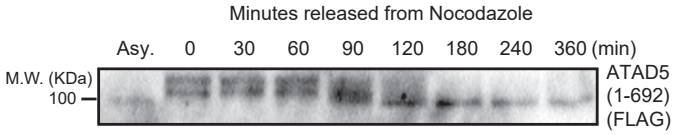

C

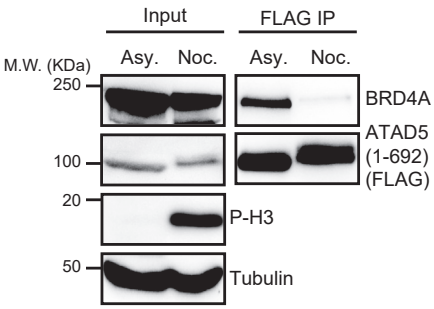

D

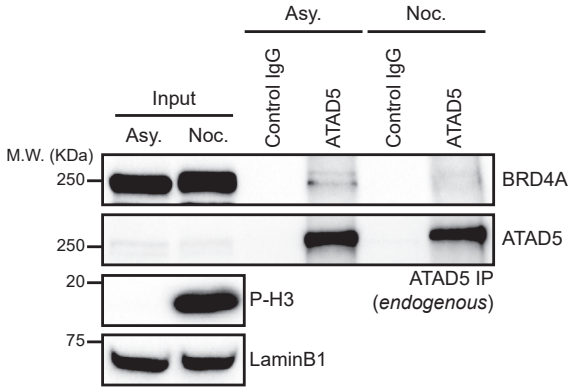

E

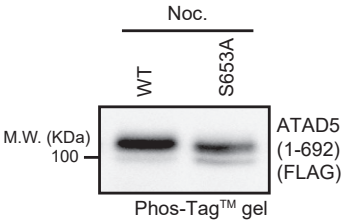

G

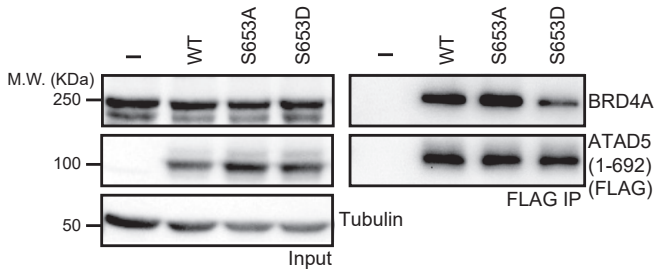

F

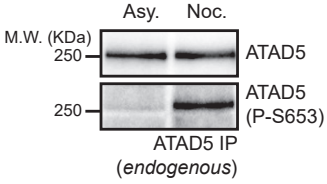

(legend on next page)

did not bind to BRD4A (Figure 2B). These results indicated that the middle region of ATAD5 (i.e., ATAD5 (400–692)) contains a BRD4-binding motif. This region is located between the UAF1-binding motif and the PCNA-unloading domain of ATAD5.

To further narrow down the candidate BRD4-binding motif, we dissected ATAD5 (400–692) (Figures 2C and S2B). ATAD5 (400–600) failed to interact with BRD4A (Figure 2C), but ATAD5 (596–692) robustly bound to BRD4A (Figure S2B). Based on those results, we defined ATAD5 (596–692) as a BET protein-binding domain (BET BD). The BET BD was predicted to form a β-stranded structure by a secondary-structure prediction program (Raptor X; Figure S2C). A β-stranded structure-forming region is well conserved among various species (Figure 2D). We mutated two conserved 3-amino acid patches in BET BD to alanine residues (top panel of Figure 2D). Those residues were predicted to be within β strands (Figure S2C). The mutations were designated as BET M1 ($E^{643}LI^{645}$ to AAA) and BET M2 ($R^{656}MK^{658}$ to AAA), respectively. BET M1, BET M2, and the combination of the two mutations, BET M12, abrogated the interaction between ATAD5 (500–692) and endogenous BRD4A (bottom panel of Figure 2D). Mutation BET M2 in full-length ATAD5 also disrupted the interaction with BRD4A (Figure 2E). Of note, polypeptide sequences around $R^{656}MK^{658}$ of ATAD5 are similar to BRD4-binding motifs of the MLV integrase, NSD3, and CHD4 (center panel of Figure 2D) (Crowe et al., 2016; Zhang et al., 2016). BRD4-binding motifs contain I/L-R/K-ϕ-R/K-ϕ (ϕ: any hydrophobic amino acid). Furthermore, it was reported that the BRD4-binding motif of the MLV integrase and NSD3 forms a β-stranded structure. Some studies showed that two negatively charged amino acid residues in the BRD4 ET domain, E653 and D655, are crucial for the binding to the MLV integrase (Crowe et al., 2016). We mutated these two residues and examined whether these mutations affect ATAD5 binding (Figure 2F). Mutation of E653 and D655 to alanine (hereafter referred to as EDAA) or positively charged amino acids (hereafter referred to as EDRK) significantly reduced the interaction between BRD4 (1–719) and ATAD5 (1–692). Full-length BRD4 (EDAA) also failed to interact with endogenous ATAD5 (Figure 2G). These results suggested that ATAD5, NSD3, CHD4, and the MLV integrase bind to the BRD4 ET domain in a similar manner. Reduced ATAD5 binding caused by the EDRK mutation in the BRD4 ET domain was not restored by a charge conversion mutation in the ATAD5 BET BD (ATAD5 (R656E K658D); Figure S2D). This finding suggested that the BRD4-ATAD5 interaction does not represent simple electrostatic interactions between charged amino acids.

To examine the intracellular interaction between ATAD5 and BRD4, we used cell-based unidentified protein interaction discovery (CUPID) analysis (Lee et al., 2011). The CUPID analysis has been used for real-time monitoring of protein–protein interactions. In CUPID, a bait protein is fused to protein kinase C-δ (PKC-δ) that migrates to the cell membrane during treatment with phorbol 12-myristate 13-acetate (PMA). A bait-binding protein comigrated with the bait-PKC-δ fusion to the cell membrane. We performed CUPID analysis with mNeongreen-ATAD5 (1–692) and PKC-δ-mRFP-BRD4B (Figures 2H and 2I). Both proteins dispersed throughout the nucleus before PMA treatment. Upon PMA treatment, ATAD5 (1–692) comigrated with PKC-δ-BRD4B to the nuclear membrane. By contrast, BET M2 ATAD5 (1–692) did not comigrate with PKC-δ-BRD4B.

To determine whether BRD4 directly interacts with ATAD5, we conducted an *in vitro* pull-down experiment with purified proteins (Figure 2J). We purified the BET BD-containing region of ATAD5, ATAD5 (500–800), and an ET domain-containing C-terminal portion of BRD4B (i.e., BRD4B (444–794)]), in a bacterial expression system. To increase stability and solubility, an MBP and a HALO tag were fused to BRD4B (444–794) and ATAD5 (500–800), respectively. Purified proteins were mixed, and then StrepII-tagged ATAD5 (500–800) was isolated using StrepTactin Sepharose beads. BRD4B (444–794) was found to be coisolated with ATAD5 (500–800). Nonetheless, mutation BET M2 in the BET BD of ATAD5 abrogated the coisolation. These data clearly showed that the BET BD of ATAD5 directly binds to the ET domain of BRD4.

Mitotic Phosphorylation Regulates the BRD4-ATAD5 Interaction

We found that ATAD5 (1–692) from nocodazole-arrested cells migrated more slowly in SDS-PAGE compared to that from G1, S, or G2 phase cells (Figures 3A and S3A). This mitotic shift of

Figure 3. Mitotic Phosphorylation of the ATAD5 BET BD Interferes with BRD4 Interaction

(A) The N-terminal domain of ATAD5 is phosphorylated in nocodazole-treated cells. Transiently expressed FLAG-ATAD5 (1–692) was FLAG purified from asynchronous or nocodazole-treated cells. Isolated proteins were analyzed by immunoblotting. Nocodazole treatment induced a mobility shift of ATAD5 (1–692) during SDS-PAGE. λ-phosphatase treatment abrogated the mobility shift.

(B) ATAD5 (1–692) was phosphorylated during mitosis. Cells stably expressing FLAG-ATAD5 (1–692) were arrested at prometaphase by nocodazole and then released. Cells were harvested at the indicated time points, and the mobility of ATAD5 (1–692) was analyzed by immunoblotting. ATAD5 (1–692) was found to be gradually dephosphorylated after the release from the nocodazole arrest.

(C) Nocodazole treatment attenuated the BRD4-ATAD5 interaction. Cells stably expressing FLAG-ATAD5 (1–692) were treated with nocodazole. ATAD5 (1–692) was FLAG immunoprecipitated, and coisolation of endogenous BRD4A was examined by immunoblotting.

(D) The interaction between endogenous ATAD5 and BRD4A is weaker during mitosis. Endogenous ATAD5 was immunoprecipitated after nocodazole treatment, and coprecipitation of endogenous BRD4A was analyzed by immunoblotting.

(E) S653 of ATAD5 is a mitotic phosphorylation site. Mutation S653A reduced the mobility shift in the Phos-Tag gel after nocodazole treatment. See Figure S3 for more information.

(F) S653 of endogenous ATAD5 is phosphorylated during mitosis. Endogenous ATAD5 was immunoprecipitated from asynchronous cells or after nocodazole treatment. S653 phosphorylation of ATAD5 was examined by anti-phospho-S653 antibody.

(G) Mitotic phosphorylation of ATAD5 S653 interferes with BRD4 binding. Wild-type, or the S653A, or the S653D mutant of FLAG-ATAD5 (1–692) was transiently expressed, and their binding to endogenous BRD4A was examined by FLAG immunoprecipitation. Phospho-mimetic mutant S653D manifested a defective BRD4 interaction.

See also Figure S3.

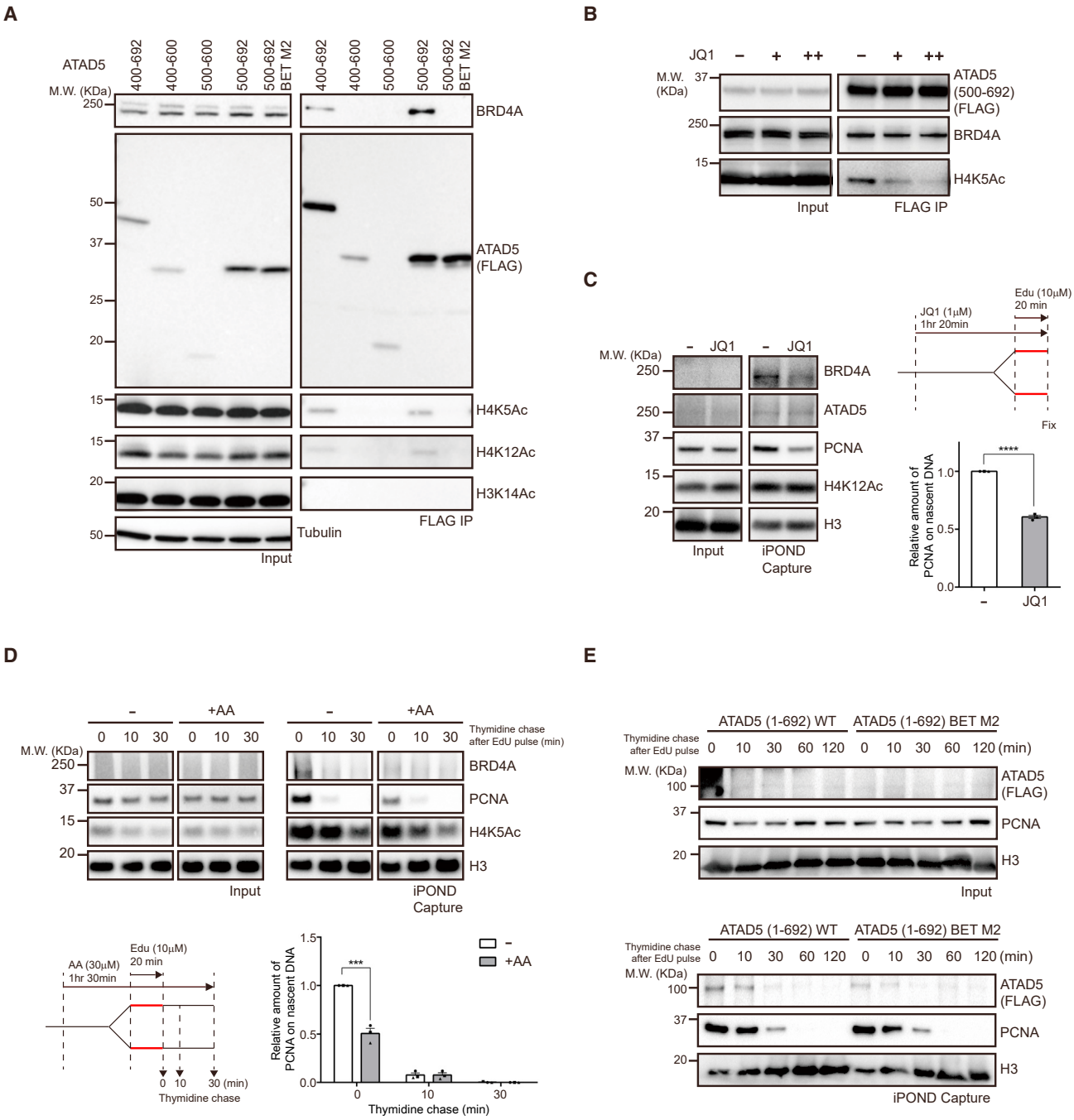

Figure 4. Acetyl-Histone-Bound BRD4 Inhibits PCNA Unloading

(A) ATAD5 (500–692) interacts with H4K5Ac and H4K12Ac in a BRD4-dependent manner. FLAG immunoprecipitation was performed on cells expressing the indicated FLAG-ATAD5 fragments. Coprecipitated endogenous BRD4A and acetyl-histones were analyzed by immunoblotting. Only BRD4-binding ATAD5 fragments copurified with H4K5Ac and H4K12Ac. See Figure S4 for more information).

(B) BRD4 inhibitor JQ1 interferes with the association of acetyl-histones with ATAD5, without affecting the BRD4-ATAD5 interaction. FLAG immunoprecipitation was performed on the lysates of cells transiently expressing FLAG-ATAD5 (500–692). Next, 0.5 μM (+) or 5 μM (++) JQ1 was applied for a 1-h incubation before harvesting.

(C) Inhibition of BRD4-acetyl-histone binding reduces the quantity of nascent chromatin-bound PCNA. JQ1 at 1 μM was added before cell harvesting, and nascent DNA-associated proteins were examined by iPOND analysis. BRD4 inhibition by JQ1 reduced the levels of BRD4 and PCNA on the nascent DNA. The nascent DNA association of ATAD5 was not affected by JQ1. A relative PCNA amount on nascent DNA was quantified from the data (n = 3, ****$p \leq 0.0001$). The error bar indicates SD.

(legend continued on next page)

ATAD5 (1–692) was abrogated by λ-phosphatase treatment. These results suggested that ATAD5 is phosphorylated upon nocodazole-induced arrest. As cells were released from the nocodazole-induced arrest, the mobility shift of ATAD5 (1–692) gradually disappeared (Figure 3B). To validate the mitosis-specific phosphorylation of ATAD5, cells harboring doxycycline-inducible ATAD5 (1–692) were arrested in the G1 phase by double-thymidine block and then released (Figure S3B). A mobility shift of ATAD5 (1–692) was observed when the amount of phospho-histone H3, a mitotic indicator, increased.

Moreover, ATAD5 (400–692) and ATAD5 (500–692), which contains the BET BD, turned out to be phosphorylated after nocodazole treatment (Figure S3C). Accordingly, we tested whether an interaction between BRD4 and ATAD5 changes during mitosis. We found that the interaction between ATAD5 (1–692) and BRD4A was significantly reduced by nocodazole treatment (Figure 3C). Immunoprecipitation of endogenous ATAD5 after the nocodazole-induced arrest also showed that the BRD4-ATAD5 interaction was attenuated by the mitotic arrest (Figure 3D).

To figure out how mitotic phosphorylation of ATAD5 inhibits the BRD4-ATAD5 interaction, we mapped mitotic phosphorylation sites in ATAD5 (Figure S3D). FLAG-ATAD5 (1–692) was affinity purified from asynchronous cells or nocodazole-arrested cells, and phosphorylation sites were identified by MS analysis. We found several phosphorylation sites specifically present in ATAD5 (1–692) in the nocodazole treatment group. Among them, the S653 residue is located in a conserved BET-protein-binding domain. To confirm the mitotic phosphorylation of S653, we prepared a phospho-dead mutant, S653A, and examined its mobility shift in a Phos-Tag gel after nocodazole treatment (Figure 3E). As expected, the S653A mutation reduced the mobility shift.

Mitotic phosphorylation of S653 was further verified with an anti-phospho-S653 antibody (Figures 3F, S3E, and S3F). The specificity of the anti-phospho-S653 antibody was validated by means of the S653A mutation (Figure S3E). S653A ATAD5 (1–692) from nocodazole-arrested cells was not recognized by the phospho-specific antibody. The anti-phospho-S653 antibody specifically detected endogenous ATAD5 that was isolated from nocodazole-arrested cells (Figure 3F). $S^{653}P^{654}$ is a putative cyclin-dependent kinase (CDK) target site. To determine whether mitotic CDK phosphorylates ATAD5, a CDK1 inhibitor (RO3306) was applied to nocodazole-arrested cells (Figure S3F). CDK1 inhibition resulted in a loss of S653 phosphorylation (Figure S3F). These data meant that the S653 residue in the BET BD of ATAD5 is phosphorylated by mitotic CDK.

Next, we determined whether S653 phosphorylation affects the BRD4-ATAD5 interaction. A phospho-mimetic S653D mutant was prepared, and its interaction with BRD4A was examined (Figure 3G). S653D mutation significantly decreased the interaction between ATAD5 and BRD4A. This result suggested that the BRD4-ATAD5 interaction is inhibited during mitosis. BET proteins may regulate ATAD5 function during interphase.

ATAD5, BRD4, and Acetyl-Histones Cooperate for Proper PCNA Unloading

BET proteins bind to acetyl-histones such as H4K5Ac and H4K12Ac through its BD. These histone marks are enriched in nascent chromatin (Figure 1B). Therefore, it is possible that BRD4, ATAD5, and acetyl-histones work together to properly unload PCNA from nascent chromatin. To test this possibility, we examined the interactions among BRD4A, ATAD5, and acetyl-histones (Figures 4A, 4B, and S4A). FLAG-tagged ATAD5 fragments were FLAG purified after transient expression (Figures 4A and S4A). The acetylation status of copurified histones was examined with antibodies that are specific for distinct acetylation marks on histone H3 or H4. We found that H4K5Ac, H4K12Ac, and H3K9Ac were enriched with ATAD5 (400–692) and ATAD5 (500–692). Enrichment of acetyl-histones was not observed with ATAD5 fragments that do not contain the BET BD. Mutation BET M2 also abrogated the coisolation of acetyl-histones. JQ1 is an inhibitor for BET proteins that interferes with the interaction between BRD4 and acetyl-histones (Filippakopoulos et al., 2010). Treatment with JQ1 significantly reduced the coisolation of H4K5Ac with FLAG-ATAD5 (500–692) without affecting the interaction between endogenous BRD4A and ATAD5 (500–692) (Figure 4B). These results suggested that ATAD5 interacts with acetyl-histone-bound BRD4A.

Next, we examined whether BRD4 regulates PCNA unloading. After JQ1 treatment, amounts of nascent DNA–bound ATAD5, BRD4A, and PCNA were monitored by iPOND analysis (Figure 4C). As expected, the amount of nascent DNA-bound BRD4A was diminished by the application of JQ1. Of note, JQ1 treatment reduced the PCNA quantity on nascent DNA. We inhibited histone acetyltransferase by anacardic acid (AA) (Figure 4D). AA decreased the amount of H4K5Ac on nascent chromatin. Downregulation of acetyl-histones by AA treatment resulted in less BRD4A association with the nascent DNA. Similar to the JQ1 treatment group, the PCNA level on nascent DNA diminished after the application of AA. These results suggested that BRD4A negatively regulates PCNA unloading on the nascent chromatin.

Because the association patterns of ATAD5 and BRD4 with nascent DNA were similar (Figure S1A), we examined whether the BRD4-ATAD5 interaction is important for the recruitment of ATAD5 to nascent chromatin. We monitored nascent DNA association with ATAD5 (1–692) BET M2 (Figure 4E) or ATAD5 (1–600) (Figure S4B). ATAD5 (1–600) lacks the BET BD. ATAD5

(D) Inhibition of histone acetyltransferase diminishes the PCNA level on the nascent DNA. EdU pulse-chase iPOND analysis was performed after anacardic acid (AA) treatment. AA treatment resulted in a reduction in the nascent DNA-associated H4K5Ac, BRD4, and PCNA. A relative PCNA amount on nascent DNA was quantified from the data (n = 3, ***$p \leq 0.001$). The error bar indicates SD.

(E) Mutation BET M2 did not significantly affect the nascent DNA association of ATAD5 (1–692). iPOND analysis was performed on cells transiently expressing either wild-type or BET M2 FLAG-ATAD5 (1–692). Endogenous ATAD5 was depleted by siRNA transfection. Cells were harvested at the indicated time points after an EdU pulse-chase procedure. Nascent DNA association of the indicated protein was analyzed by immunoblotting.

See also Figure S4.

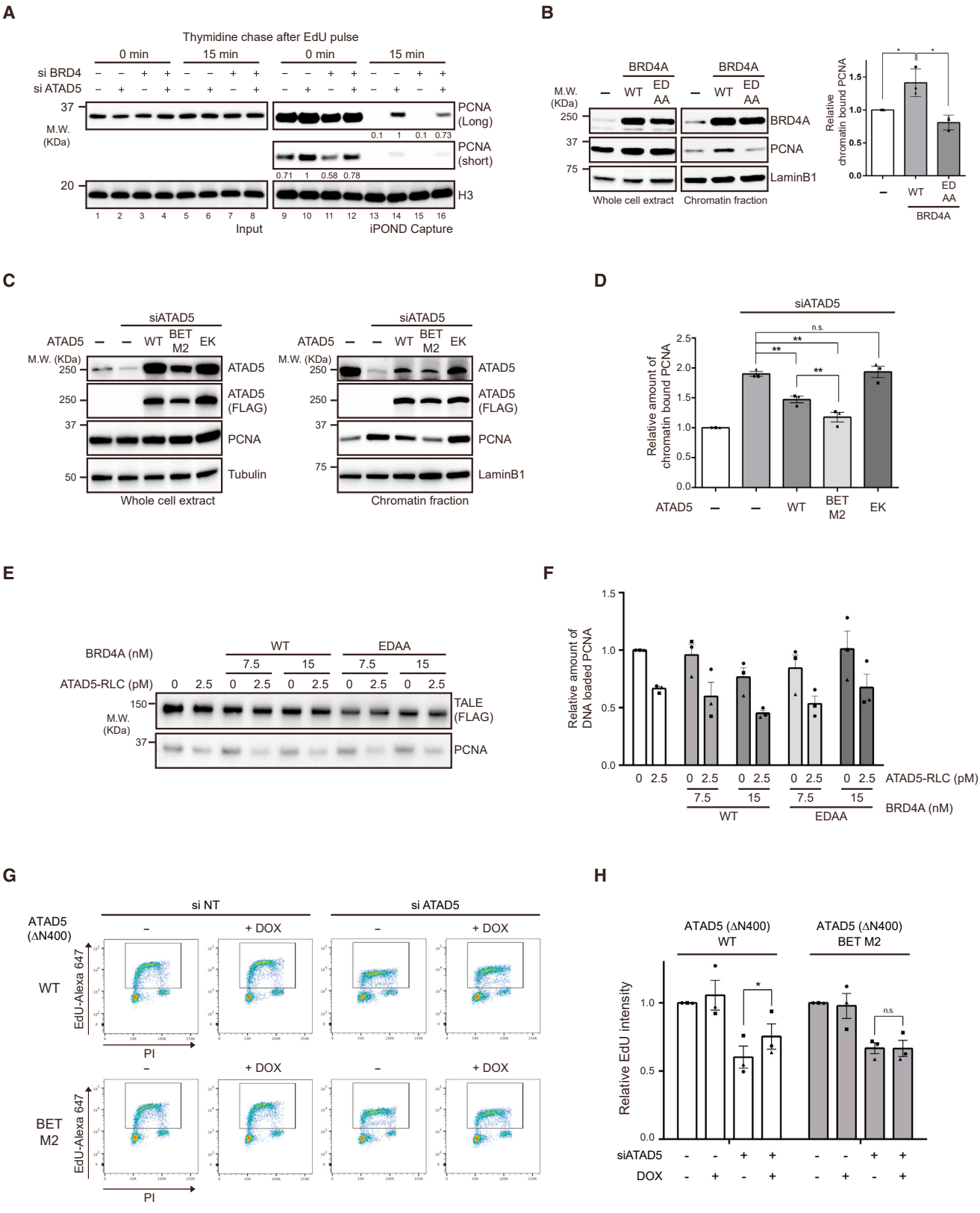

(legend on next page)

associated with nascent DNA regardless of its BRD4-binding ability. Therefore, an interaction with BRD4 is not necessary for nascent DNA association of ATAD5.

The BRD4 Fine-Tunes PCNA Unloading by ATAD5-RLC

If BRD4A inhibits PCNA unloading from nascent chromatin, then BRD4A depletion should reduce the accumulation of PCNA in chromatin. To examine this possibility, we monitored the PCNA level on nascent DNA after a knockdown of ATAD5 and BRD4A. Because ATAD5-RLC is a major PCNA unloader (Kang et al., 2019), ATAD5 depletion increased the PCNA quantity on nascent DNA. Furthermore, the ATAD5 knockdown delayed PCNA dissociation from nascent DNA (compare lanes 9 and 13 with lanes 10 and 14 in Figure 5A). However, depletion of BRD4A slightly reduced the binding of PCNA to nascent DNA (compare lane 9 with lane 11 in Figure 5A). A double knockdown of BRD4A and ATAD5 more clearly showed the inhibitory action of BRD4 on PCNA unloading (compare lanes 10 and 14 with lanes 12 and 16 in Figure 5A). Co-depletion of BRD4A and ATAD5 resulted in more rapid dissociation of PCNA from nascent DNA as compared to ATAD5 depletion alone. These results implied that BRD4A negatively controls PCNA unloading from nascent DNA.

Next, we examined the effect of BRD4A overexpression on PCNA unloading (Figure 5B). Transfection of BRD4A significantly increased the amount of BRD4A both in the whole-cell extract and in a chromatin fraction. Of note, the overexpression of BRD4A increased the amount of chromatin-bound PCNA. In contrast, an ET domain mutant of BRD4A—BRD4A (EDAA)—did not induce the accumulation of PCNA in chromatin. These results also support the notion that BRD4 inhibits PCNA unloading through its interaction with ATAD5.

As previously reported, the add-back of exogenous ATAD5 into ATAD5-depleted cells reduced the chromatin-bound PCNA amount (Figures 5C and 5D). ATAD5 (E1173K, EK) is an ATPase motif mutant and is deficient in PCNA unloading (Kang et al., 2019). Accordingly, the expression of ATAD5 (E1173K) in ATAD5-depleted cells failed to decrease the chromatin-accumulated PCNA amount. The add-back of ATAD5 (BET M2) more strongly diminished the chromatin-accumulated PCNA amount as compared to the wild-type add-back group. This result also supports the notion that BRD4A binds to ATAD5 and inhibits the PCNA-unloading activity of ATAD5-RLC.

To test whether the binding of BRD4A directly inhibits ATAD5-RLC, we performed an *in vitro* PCNA-unloading assay (Figures 5E, 5F, and S5B) (Kang et al., 2019). PCNA was loaded onto bead-coupled substrate DNA using purified RFC. Substrate DNA was a 130-mer that contained a 10-nt gap. The free end of DNA was blocked by transcription activator-like effector (TALE)-protein binding to prevent a slide-off of DNA-loaded PCNA. ATAD5-RLC unloaded PCNA, as reported previously (Figures 5E and 5F). We purified wild-type BRD4A and BRD4A (EDAA) (Figure S5B) to examine their effect on PCNA unloading. BRD4 did not inhibit PCNA unloading *in vitro* (Figures 5E and 5F). These data suggested that the inhibition of PCNA unloading by BRD4 may require acetyl-histone association with BRD4-ATAD5.

Next, we determined whether the ATAD5-BRD4 interaction affects DNA replication. We prepared HeLa cell lines that harbor doxycycline-inducible wild-type or BET M2 ATAD5 (ΔN400). ATAD5 (ΔN400) contains both the BET BD and PCNA-unloading domain (Kang et al., 2019). Endogenous ATAD5 was depleted by small interfering RNA (siRNA) transfection, and doxycycline was applied to turn on ATAD5 (ΔN400). DNA replication of each sample was monitored by a 5-ethynyl-2′-deoxyuridine (EdU) incorporation assay (Figures 5G, 5H, and S5C). As reported elsewhere, ATAD5 depletion reduced EdU incorporation. Wild-type ATAD5 (ΔN400) partially reversed the decrease in EdU incorporation, but the BET M2 mutant did so less efficiently. These results suggested that BRD4-mediated fine-tuning of PCNA unloading facilitates DNA replication.

DISCUSSION

Chromatin status influences DNA replication initiation. The BAH domain of origin recognition complex 1 (ORC1) facilitates chromatin binding of the ORC (Kuo et al., 2012). BRD4 recruits TICRR to euchromatin and facilitates origin firing (Sansam et al., 2018). In addition, a chromatin landscape influences multiple steps of replication initiation *in vitro* (Azmi et al., 2017). Here, we

Figure 5. BRD4 Fine-Tunes the PCNA-Unloading Activity of ATAD5-RLC

(A) BRD4 depletion enhances PCNA unloading by ATAD5-RLC. After depletion of ATAD5 and/or BRD4A, EdU pulse-chase iPOND was performed. PCNA on the nascent DNA was quantified by immunoblotting. The amount of nascent DNA-associated PCNA decreased after BRD4 depletion. Numbers below PCNA blots indicate the relative amount of PCNA.

(B) BRD4 inhibits PCNA unloading. After transient overexpression of either wild-type BRD4A or BRD4A (EDAA), chromatin-bound PCNA was analyzed. Wild-type BRD4A induced the accumulation of PCNA on chromatin, but BRD4A (EDAA) did not. A relative PCNA amount on chromatin was quantified from the data ($n = 3$, $^{*}p < 0.05$). The error bar indicates SD.

(C) BET M2 mutant ATAD5 more robustly unloads PCNA as compared to the wild type. Wild-type, BET M2, or E1173K mutant ATAD5 was transiently expressed in endogenous ATAD5-depleted cells. After chromatin fractionation, chromatin-bound PCNA was analyzed by immunoblotting. Blots of a whole-cell extract are presented as a control. Less PCNA was observed on the chromatin of BET M2 mutant-expressing cells compared to the wild-type group.

(D) A relative PCNA amount on chromatin was quantified from the data in (C) ($n = 3$, $^{**}p \leq 0.01$). The error bar indicates SD.

(E) The influence of BRD4A on PCNA unloading *in vitro*. A PCNA-unloading assay was performed with ATAD5-RLC in the presence of purified wild-type BRD4A or BRD4A (EDAA). PCNA-unloading activity of ATAD5-RLC was not inhibited by BRD4A *in vitro*.

(F) Quantification of DNA-bound PCNA from the data in (E) ($n = 3$). The error bar indicates SD.

(G) BRD4-ATAD5 interaction is important for DNA replication. Cells harboring doxycycline-inducible wild-type or BET M2 ATAD5 (ΔN400) were used in this experiment. Endogenous ATAD5 was depleted by siRNA transfection, and ATAD5 (ΔN400) was turned on by doxycycline. Cells were EdU pulse labeled, and EdU incorporation was monitored by flow cytometry. Rectangles indicate the regions for quantification.

(H) Quantification of data in (G) ($n = 3$, $^{*}p < 0.05$). The error bar indicates SD.

See also Figure S5.

demonstrated that chromatin also affects the later stage of DNA replication: PCNA unloading.

PCNA is especially crucial for discontinuous lagging-strand synthesis. Therefore, PCNA must be continuously loaded onto the lagging-strand template. In contrast, PCNA that is accumulated on the nascent DNA must be unloaded. Considering the amount of Okazaki fragments that are synthesized during S phase, recycling of PCNA is required to support efficient genome duplication. PCNA unloading is also important for the completion of chromosome replication. PCNA molecules that stay between nucleosomes could interfere with nascent chromatin organization. Therefore, PCNA unloading must be finely regulated because PCNA is crucial both for Okazaki fragment maturation and for nucleosome deposition. Previously, we showed that replication proteins can inhibit ATAD5-RLC *in vitro* to prevent premature PCNA unloading before Okazaki fragment maturation (Kang et al., 2019). The present study revealed another regulatory mechanism for PCNA unloading. Acetyl-histone-bound BRD4 negatively regulates ATAD5-dependent PCNA unloading (Figures 4 and 5). BRD4 may function as a safety break that keeps ATAD5-RLC inactive until PCNA accomplishes its task on nascent DNA. The BRD4-binding domain, BET BD, is located immediately upstream of the PCNA-unloading domain of ATAD5. To open and unload a PCNA ring, the pentameric surface of ATAD5-RLC binds to the front face of a PCNA homotrimer. The interaction between acetyl-histone-bound BRD4 and ATAD5 may interfere with the access of ATAD5-RLC to PCNA.

The ATAD5 BET BD bound to the ET domain of BRD4 (Figures 2 and 3). In addition to ATAD5, BRD4 interacts with many proteins through the ET domain. Our results indicate that the BET BD of ATAD5 is similar to that of known ET-binding proteins. Therefore, ATAD5 and other ET-binding proteins cannot bind to a BRD4 molecule at the same time. The BRD4-ATAD5-RLC complex may function as a discrete unit that regulates timely PCNA unloading. The interaction between BRD4 and ATAD5 was weakened by mitotic phosphorylation of the ATAD5 BET BD. Without BRD4 binding, ATAD5-RLC could efficiently unload PCNA from a mitotic chromosome. Otherwise, separation of BRD4 and ATAD5 may be required for the mitotic function of each protein.

Newly synthesized histones, which are deposited on nascent DNA, undergo acetylation at lysines 5 and 12 (histone H4) in mammalian cells. It has been suggested that these acetylated sites facilitate nucleosome deposition on nascent DNA. Because H4K5Ac and H4K12Ac amounts decrease as a replication fork progresses (Figure 1B), these acetylated sites specifically mark the nascent chromatin. On the nascent DNA, PCNA unloading must be coordinated with chromatin organization. H4K5Ac and H4K12Ac may be docking sites for chromatin-binding proteins that bridge PCNA unloading and chromatin status. We propose that the BRD4-ATAD5 complex engages in cross-talk with the acetyl-histone marks on nascent DNA to fine-tune PCNA unloading (Figure S5D). BRD4 was localized to nascent DNA through binding to acetyl-histones (Figures 4C and S1A). ATAD5 also migrated to nascent DNA (Figures 1 and 4). It remains to be elucidated how ATAD5 is recruited to the sites of DNA synthesis. BRD4 binding seems to be unnecessary for the recruitment of ATAD5 to nascent DNA. Once there, BRD4 binds to ATAD5-RLC and inhibits PCNA unloading (Figures 4 and 5). As a replication fork proceeds, H4K5Ac and H4K12Ac are deacetylated, and BRD4 is released from the nascent chromatin. The BRD4 release can activate ATAD5-RLC for PCNA unloading. As we reported previously, ATAD5-RLC is released from DNA with PCNA during unloading (Kang et al., 2019). During the inhibition of ATAD5-RLC, PCNA remains on nascent DNA and aids in the early steps of nascent chromatin assembly. Our study provides intriguing insight into how epigenetic information affects the activity of replication machinery on nascent DNA.

STAR★METHODS

Detailed methods are provided in the online version of this paper and include the following:

- KEY RESOURCES TABLE
- LEAD CONTACT AND MATERIALS AVAILABILITY
- EXPERIMENTAL MODEL AND SUBJECT DETAILS
  - Cell culture and cell lines
- METHOD DETAILS
  - Plasmid and siRNA transfection
  - Plasmids
  - siRNAs
  - iPOND
  - Immunoprecipitation and western blot analysis
  - Antibodies
  - AP-MS analysis
  - CUPID analysis
  - Protein purification
  - An *in vitro* pull-down assay
  - Chromatin fractionation
  - The PCNA-unloading reaction
  - An EdU incorporation assay
- QUANTIFICATION AND STATISTICAL ANALYSIS
- DATA AND CODE AVAILABILITY

SUPPLEMENTAL INFORMATION

Supplemental Information can be found online at https://doi.org/10.1016/j.celrep.2019.11.114.

ACKNOWLEDGMENTS

We thank members of the Center for Genomic Integrity, IBS, for helpful discussions and comments on the manuscript. We thank Seong-Jung Kim for providing the anti-phospho-S653 antibody. The pmRFP-PKC-δ plasmid for the CUPID analysis was kindly provided by PROBON BIO. E.R. and Y.J.K. were supported by Global PhD Fellowships (NRF-2017H1A2A1044961 and NRF-2018H1A2A1063189, respectively). This research was mainly supported by the Institute for Basic Science (IBS-R022-D1). This work was also partially supported by the UNIST research fund (1.180063).

AUTHOR CONTRIBUTIONS

M.-S.K. and J.K. conducted most of the experiments. E.R. purified the proteins and performed the *in vitro* PCNA unloading assay. N.Y.H. generated the DNA constructs for this study and performed the sample preparation for the MS analysis. S.H. conducted the iPOND analysis. B.-G.K. performed the MS analysis. J.S.R. performed the flow cytometry analysis. Y.J.K. conducted several

immunoprecipitation experiments. J.M.H. assisted with the CUPID analysis. M.-S.K., J.K., E.R., and S.K. designed the experiments and analyzed the data. S.K. drafted the manuscript with input from all of the authors. S.K. and K.M. supervised the project.

DECLARATION OF INTERESTS

The authors declare no competing interests.

Received: June 26, 2019
Revised: November 1, 2019
Accepted: November 27, 2019
Published: December 24, 2019

REFERENCES

Azmi, I.F., Watanabe, S., Maloney, M.F., Kang, S., Belsky, J.A., MacAlpine, D.M., Peterson, C.L., and Bell, S.P. (2017). Nucleosomes influence multiple steps during replication initiation. eLife *6*, e22512.

Crowe, B.L., Larue, R.C., Yuan, C., Hess, S., Kvaratskhelia, M., and Foster, M.P. (2016). Structure of the Brd4 ET domain bound to a C-terminal motif from γ-retroviral integrases reveals a conserved mechanism of interaction. Proc. Natl. Acad. Sci. USA *113*, 2086–2091.

Donati, B., Lorenzini, E., and Ciarrocchi, A. (2018). BRD4 and cancer: going beyond transcriptional regulation. Mol. Cancer *17*, 164.

Filippakopoulos, P., Qi, J., Picaud, S., Shen, Y., Smith, W.B., Fedorov, O., Morse, E.M., Keates, T., Hickman, T.T., Felletar, I., et al. (2010). Selective inhibition of BET bromodomains. Nature *468*, 1067–1073.

Floyd, S.R., Pacold, M.E., Huang, Q., Clarke, S.M., Lam, F.C., Cannell, I.G., Bryson, B.D., Rameseder, J., Lee, M.J., Blake, E.J., et al. (2013). The bromodomain protein Brd4 insulates chromatin from DNA damage signalling. Nature *498*, 246–250.

Gali, V.K., Dickerson, D., Katou, Y., Fujiki, K., Shirahige, K., Owen-Hughes, T., Kubota, T., and Donaldson, A.D. (2018). Identification of Elg1 interaction partners and effects on post-replication chromatin re-formation. PLoS Genet. *14*, e1007783.

Jang, M.K., Mochizuki, K., Zhou, M., Jeong, H.S., Brady, J.N., and Ozato, K. (2005). The bromodomain protein Brd4 is a positive regulatory component of P-TEFb and stimulates RNA polymerase II-dependent transcription. Mol. Cell *19*, 523–534.

Jones, D.H., and Lin, D.I. (2017). Amplification of the *NSD3-BRD4-CHD8* pathway in pelvic high-grade serous carcinomas of tubo-ovarian and endometrial origin. Mol. Clin. Oncol. *7*, 301–307.

Kang, S., Kang, M.S., Ryu, E., and Myung, K. (2018). Eukaryotic DNA replication: orchestrated action of multi-subunit protein complexes. Mutat. Res. *809*, 58–69.

Kang, M.-S., Ryu, E., Lee, S.-W., Park, J., Ha, N.Y., Ra, J.S., Kim, Y.J., Kim, J., Abdel-Rahman, M., Park, S.H., et al. (2019). Regulation of PCNA cycling on replicating DNA by RFC and RFC-like complexes. Nat. Commun. *10*, 2420.

Konuma, T., Yu, D., Zhao, C., Ju, Y., Sharma, R., Ren, C., Zhang, Q., Zhou, M.M., and Zeng, L. (2017). Structural Mechanism of the Oxygenase JMJD6 Recognition by the Extraterminal (ET) Domain of BRD4. Sci. Rep. *7*, 16272.

Korb, E., Herre, M., Zucker-Scharff, I., Gresack, J., Allis, C.D., and Darnell, R.B. (2017). Excess Translation of Epigenetic Regulators Contributes to Fragile X Syndrome and Is Alleviated by Brd4 Inhibition. Cell *170*, 1209–1223.e20.

Kuo, A.J., Song, J., Cheung, P., Ishibe-Murakami, S., Yamazoe, S., Chen, J.K., Patel, D.J., and Gozani, O. (2012). The BAH domain of ORC1 links H4K20me2 to DNA replication licensing and Meier-Gorlin syndrome. Nature *484*, 115–119.

Kurat, C.F., Yeeles, J.T.P., Patel, H., Early, A., and Diffley, J.F.X. (2017). Chromatin Controls DNA Replication Origin Selection, Lagging-Strand Synthesis, and Replication Fork Rates. Mol. Cell *65*, 117–130.

Lee, K.Y., Yang, K., Cohn, M.A., Sikdar, N., D'Andrea, A.D., and Myung, K. (2010). Human ELG1 regulates the level of ubiquitinated proliferating cell nuclear antigen (PCNA) through its interactions with PCNA and USP1. J. Biol. Chem. *285*, 10362–10369.

Lee, K.B., Hwang, J.M., Choi, I.S., Rho, J., Choi, J.S., Kim, G.H., Kim, S.I., Kim, S., and Lee, Z.W. (2011). Direct monitoring of the inhibition of protein-protein interactions in cells by translocation of PKCδ fusion proteins. Angew. Chem. Int. Engl. *50*, 1314–1317.

Lee, K.Y., Fu, H., Aladjem, M.I., and Myung, K. (2013). ATAD5 regulates the lifespan of DNA replication factories by modulating PCNA level on the chromatin. J. Cell Biol. *200*, 31–44.

Li, X., Baek, G., Ramanand, S.G., Sharp, A., Gao, Y., Yuan, W., Welti, J., Rodrigues, D.N., Dolling, D., Figueiredo, I., et al. (2018). BRD4 Promotes DNA Repair and Mediates the Formation of TMPRSS2-ERG Gene Rearrangements in Prostate Cancer. Cell Rep. *22*, 796–808.

Liu, W., Ma, Q., Wong, K., Li, W., Ohgi, K., Zhang, J., Aggarwal, A., and Rosenfeld, M.G. (2013). Brd4 and JMJD6-associated anti-pause enhancers in regulation of transcriptional pause release. Cell *155*, 1581–1595.

Lopez-Contreras, A.J., Ruppen, I., Nieto-Soler, M., Murga, M., Rodriguez-Acebes, S., Remeseiro, S., Rodrigo-Perez, S., Rojas, A.M., Mendez, J., Muñoz, J., and Fernandez-Capetillo, O. (2013). A proteomic characterization of factors enriched at nascent DNA molecules. Cell Rep. *3*, 1105–1116.

Loyola, A., Bonaldi, T., Roche, D., Imhof, A., and Almouzni, G. (2006). PTMs on H3 variants before chromatin assembly potentiate their final epigenetic state. Mol. Cell *24*, 309–316.

Maruyama, T., Farina, A., Dey, A., Cheong, J., Bermudez, V.P., Tamura, T., Sciortino, S., Shuman, J., Hurwitz, J., and Ozato, K. (2002). A mammalian bromodomain protein, brd4, interacts with replication factor C and inhibits progression to S phase. Mol. Cell. Biol. *22*, 6509–6520.

Moldovan, G.L., Pfander, B., and Jentsch, S. (2007). PCNA, the maestro of the replication fork. Cell *129*, 665–679.

Petryk, N., Dalby, M., Wenger, A., Stromme, C.B., Strandsby, A., Andersson, R., and Groth, A. (2018). MCM2 promotes symmetric inheritance of modified histones during DNA replication. Science *361*, 1389–1392.

Poot, R.A., Bozhenok, L., van den Berg, D.L., Steffensen, S., Ferreira, F., Grimaldi, M., Gilbert, N., Ferreira, J., and Varga-Weisz, P.D. (2004). The Williams syndrome transcription factor interacts with PCNA to target chromatin remodelling by ISWI to replication foci. Nat. Cell Biol. *6*, 1236–1244.

Reveron-Gomez, N., Gonzalez-Aguilera, C., Stewart-Morgan, K.R., Petryk, N., Flury, V., Graziano, S., Johansen, J.V., Jakobsen, J.S., Alabert, C., and Groth, A. (2018). Accurate Recycling of Parental Histones Reproduces the Histone Modification Landscape during DNA Replication. Mol. Cell *72*, 239–249e.5.

Sabari, B.R., Dall'Agnese, A., Boija, A., Klein, I.A., Coffey, E.L., Shrinivas, K., Abraham, B.J., Hannett, N.M., Zamudio, A.V., Manteiga, J.C., et al. (2018). Coactivator condensation at super-enhancers links phase separation and gene control. Science *361*, eaar3958.

Sansam, C.G., Pietrzak, K., Majchrzycka, B., Kerlin, M.A., Chen, J., Rankin, S., and Sansam, C.L. (2018). A mechanism for epigenetic control of DNA replication. Genes Dev. *32*, 224–229.

Shen, C., Ipsaro, J.J., Shi, J., Milazzo, J.P., Wang, E., Roe, J.S., Suzuki, Y., Pappin, D.J., Joshua-Tor, L., and Vakoc, C.R. (2015). NSD3-Short Is an Adaptor Protein that Couples BRD4 to the CHD8 Chromatin Remodeler. Mol. Cell *60*, 847–859.

Shibahara, K., and Stillman, B. (1999). Replication-dependent marking of DNA by PCNA facilitates CAF-1-coupled inheritance of chromatin. Cell *96*, 575–585.

Sirbu, B.M., Couch, F.B., Feigerle, J.T., Bhaskara, S., Hiebert, S.W., and Cortez, D. (2011). Analysis of protein dynamics at active, stalled, and collapsed replication forks. Genes Dev. *25*, 1320–1327.

Sobel, R.E., Cook, R.G., Perry, C.A., Annunziato, A.T., and Allis, C.D. (1995). Conservation of deposition-related acetylation sites in newly synthesized histones H3 and H4. Proc. Natl. Acad. Sci. USA *92*, 1237–1241.

Sun, C., Yin, J., Fang, Y., Chen, J., Jeong, K.J., Chen, X., Vellano, C.P., Ju, Z., Zhao, W., Zhang, D., et al. (2018). BRD4 Inhibition Is Synthetic Lethal with

PARP Inhibitors through the Induction of Homologous Recombination Deficiency. Cancer Cell *33*, 401–416.e8.

White, M.E., Fenger, J.M., and Carson, W.E., 3rd. (2019). Emerging roles of and therapeutic strategies targeting BRD4 in cancer. Cell. Immunol. *337*, 48–53.

Yang, Z., Yik, J.H., Chen, R., He, N., Jang, M.K., Ozato, K., and Zhou, Q. (2005). Recruitment of P-TEFb for stimulation of transcriptional elongation by the bromodomain protein Brd4. Mol. Cell *19*, 535–545.

Yu, C., Gan, H., Serra-Cardona, A., Zhang, L., Gan, S., Sharma, S., Johansson, E., Chabes, A., Xu, R.M., and Zhang, Z. (2018). A mechanism for preventing asymmetric histone segregation onto replicating DNA strands. Science *361*, 1386–1389.

Zhang, Z., Shibahara, K., and Stillman, B. (2000). PCNA connects DNA replication to epigenetic inheritance in yeast. Nature *408*, 221–225.

Zhang, Q., Zeng, L., Shen, C., Ju, Y., Konuma, T., Zhao, C., Vakoc, C.R., and Zhou, M.M. (2016). Structural Mechanism of Transcriptional Regulator NSD3 Recognition by the ET Domain of BRD4. Structure *24*, 1201–1208.

STAR★METHODS

KEY RESOURCES TABLE

REAGENT or RESOURCE	SOURCE	IDENTIFIER
Antibodies		
Mouse monoclonal anti FLAG M2	Sigma-Aldrich	Cat#F3165; RRID: AB_259529
Mouse monoclonal anti PCNA	Santa Cruz Biotechnology	Cat#sc-56; RRID: AB_628110
Acetyl Histone H3 antibody sampler kit	Cell Signaling Technology	Cat#9927
Acetyl Histone H4 antibody set	Merck-Millipore	Cat#17-211
Rabbit polyclonal anti Histone H3, CT, pan	Merck-Millipore	Cat#07-690; RRID: AB_417398
Rabbit polyclonal anti BRD2	Bethyl	Cat#A302-583A; RRID: AB_2034829
Rabbit polyclonal anti BRD3	Bethyl	Cat#A302-368A; RRID: AB_1907251
Rabbit polyclonal anti BRD4	Bethyl	Cat#A301-985A; RRID: AB_1576498
Rabbit polyclonal anti pan BRD4	Sigma-Aldrich	Cat#AV39076; RRID: AB_1845434
Rabbit polyclonal anti V5	Sigma-Aldrich	Cat#V8137; RRID: AB_261889
Mouse monoclonal anti WDR48 (UAF1)	Santa Cruz Biotechnology	Cat#sc-514473
Mouse monoclonal anti S tag	Sigma-Aldrich	Cat#SAB2702227
Mouse monoclonal anti phospho Histone H3 (Ser10)	Cell Signaling Technology	Cat#9706; RRID: AB_331748
Rabbit polyclonal anti Beta Tubulin	Abcam	Cat#ab15568; RRID: AB_2210952
Rabbit polyclonal anti Lamin B1	Abcam	Cat#ab16048; RRID: AB_10107828
Mouse monoclonal anti Histone H2A.X, phospho (Ser139)	Merck-Millipore	Cat#05-636; RRID: AB_309864
Rabbit anti human ATAD5	Lee et al., 2010	N/A
Rabbit anti human ATAD5, phospho (Ser653)	This paper	N/A
Chemicals, Peptides, and Recombinant Proteins		
3xFLAG peptide	Sigma-Aldrich	Cat#F4799
Desthiobiotin	Sigma-Aldrich	Cat#D1411
Edu	Invitrogen	Cat#E10187
Thymidine	Sigma-Aldrich	Cat#T1895
Phorbol 12-myristate 13-acetate (PMA)	Sigma-Aldrich	Cat#P8139
Hydroxyurea (HU)	Sigma-Aldrich	Cat#H8627
Methyl methane sulfonate (MMS)	Sigma-Aldrich	Cat#129925
Nocodazole	Sigma-Aldrich	Cat#M1404
Lambda protein phosphatase (Lambda PP)	New England Biolabs	Cat#P0753
Phos-tag™ acrylamide	NARD Institute, LTD.	Cat#AAL-107
Cdk1 inhibitor (RO-3306)	Sigma-Aldrich	Cat#SML0569
JQ1	Sigma-Aldrich	Cat#SML0974
Anacardic acid	Sigma-Aldrich	Cat#A7236
Critical Commercial Assays		
Click-iT™ Plus EdU Alexa Fluor™ 647 Flow Cytometry Assay Kit	Invitrogen	Cat#C10635
Deposited data		
ATAD5 (1-692) interactome	This paper	ProteomeXchange: PXD016309
Experimental Models: Cell Lines		
HEK293T	ATCC	Cat#CRL-11268; RRID: CVCL_1926
HeLa	ATCC	Cat#CCL-2; RRID: CVCL_0030

(*Continued on next page*)

Continued

REAGENT or RESOURCE	SOURCE	IDENTIFIER
Oligonucleotides		
BRD4A siRNA sense	Floyd et al., 2013	N/A
5′-GGGAGAAAGAGGAGCGUGAUU-3′		
BRD4A siRNA antisense	Floyd et al., 2013	N/A
5′-AAUCACGCUCCUCUUUCUCCC-3′		
BRD4B siRNA sense	Floyd et al., 2013	N/A
5′- GCACCAGUGGAGACUUCGUUU-3′		
BRD4B siRNA antisense	Floyd et al., 2013	N/A
5′- AAACGAAGUCUCCACUGGUGC-3′		
Pan BRD4 siRNA	Invitrogen	Cat#1299001
ATAD5 siRNA sense	Lee et al., 2010	N/A
5′- GUAUAUUUCUCGAUGUACAUU 3′		
ATAD5 siRNA antisense	Lee et al., 2010	N/A
5′- UGUACAUCGAGAAAUAUACUU −3′		
AccuTarget™ Negative Control siRNA	Bioneer	N/A
Recombinant DNA		
GFP-BRD2 plasmid	Addgene	Addgene Cat#65376
GFP-BRD3 plasmid	Addgene	Addgene Cat#65377
HA-BRD4 plasmid	Addgene	Addgene Cat#31351
Software and Algorithms		
Raptor X web server (structure prediction)	Jinbo Xu group	http://raptorx.uchicago.edu/StructPredV2/predict/
ZEN (blue edition)	Carl Zeiss	https://www.zeiss.com/microscopy/int/products/microscope-software.html
FlowJo	Tree Star	https://www.flowjo.com/solutions/flowjo/; RRID: SCR_008520
GraphPad Prism	GraphPad Software	https://www.graphpad.com/scientific-software/prism/; RRID: SCR_000306

LEAD CONTACT AND MATERIALS AVAILABILITY

Further information and requests for resources should be directed to and will be fulfilled by the Lead Contact, Dr. Sukhyun Kang (kangsh@ibs.re.kr). Plasmids generated in this study are available upon request. No other unique reagents were generated.

EXPERIMENTAL MODEL AND SUBJECT DETAILS

Cell culture and cell lines

Human HEK293T cells (purchased from American Type Culture Collection; Manassas, VA) was cultured in Dulbecco's modified Eagle's medium (Hyclone) supplemented with 10% of fetal bovine serum (Hyclone) and 1% of a penicillin-streptomycin solution (GIBCO) at 37°C and 5% CO_2. HeLa-derived cell lines that stably express FLAG-tagged ATAD5 proteins were generated by means of a Flp-In™ system (Thermo Fisher Scientific). Tetracycline-free serum was used for the maintenance of the stable cell lines carrying a doxycycline-inducible construct. To synchronize cells in the G1 phase, double thymidine block was performed. Cells were treated with 2.5 mM thymidine for 17 h. The cells were washed with PBS, and the culture was continued in the regular medium for 10 h. The cells were treated again with 2.5 mM thymidine for 17 h and washed with PBS. Arrested cells were released from the G1 phase by cultivation in the regular growth medium. HEK293T and HeLa cells are female.

METHOD DETAILS

Plasmid and siRNA transfection

HEK293T cells were transiently transfected with various plasmids using the X-tremeGENE™ HP DNA Transfection Reagent (Roche). For a protein knockdown, cells were transfected with various siRNAs via Lipofectamine RNAiMAX (Thermo Fisher Scientific). Plasmid- or siRNA-transfected cells were harvested 48 h after transfection for further analysis.

Plasmids

Wild-type ATAD5 or BRD4 and its mutants were cloned into the p3 × FLAG-CMV10 expression vector (Sigma-Aldrich), pcDNA5/FRT/TO (Thermo Fisher Scientific), or pcDNA3.1 (Invitrogen). All constructs were confirmed by sequencing. The plasmids used in this work are listed in Table S1. Point mutations were introduced by site-directed mutagenesis with the QuikChange Site-Directed Mutagenesis Kit (Agilent Technologies).

siRNAs

BRD4A siRNAs with sequences 5′-GGGAGAAAGAGGAGCGUGAUU-3′ (sense) and 5′-AAUCACGCUCCUCUUUCUCCC-3′ (antisense), BRD4B siRNAs with sequences 5′- GCACCAGUGGAGACUUCGUUU-3′ (sense) and 5′- AAACGAAGUCUCCACUGG UGC-3′ (antisense), and siRNAs specific to the 3′ untranslated region (UTR) of ATAD5 mRNA with sequences 5′- GUAUAUUUCUC GAUGUACAUU-3′ (sense) and 5′- UGUACAUCGAGAAAUAUACUU-3′ (antisense) were synthesized by Bioneer (South Korea). Non-targeting control siRNA (AccuTarget Negative Control siRNA) and Pan-BRD4 siRNAs (siRNA ID: HSS141059) were purchased from Bioneer (South Korea) and Invitrogen, respectively.

iPOND

iPOND was performed as described by Sirbu et al. (2011) with slight modifications. Briefly, HEK293T cells were pulsed with a medium containing EdU (10 μM, Life Technologies) for 20 min. The EdU-labeled cells were washed once with a medium containing 10 μM thymidine to remove EdU, then a thymidine chase was performed with a medium containing 10 μM thymidine for 0, 10, 30, 60, or 120 min. Cells were cross-linked with 1% formaldehyde for 20 min at room temperature, quenched with 0.125 M glycine, and washed with PBS. For the conjugation of EdU with biotin azide, cells were permeabilized with 0.25% Triton X-100/ PBS and incubated in click reaction buffer (10 mM sodium-L-ascorbate, 20 μM biotin azide (Life Technologies), and 2 mM $CuSO_4$) for 30 min at room temperature. After centrifugation, the pellets were washed once with 0.5% BSA/PBS and twice with PBS. The cells were resuspended in lysis buffer (50 mM Tris-HCl pH 8.0, and 1% of SDS) supplemented with protease inhibitors and were sonicated. The lysates were cleared and then incubated with streptavidin-agarose beads (Novagen) overnight at 4°C. The beads were washed once with lysis buffer, once with 1 M NaCl, and then twice with lysis buffer. To elute proteins bound to nascent DNA, 2 × SDS Laemmli sample buffer was added to packed beads (1:1; v/v). Samples were incubated at 95°C for 30 min, loaded on a gel for SDS-PAGE, and analyzed by immunoblotting.

Immunoprecipitation and western blot analysis

Whole-cell lysates were extracted with buffer X (100 mM Tris-HCl pH 8.5, 250 mM NaCl, 1 mM EDTA, 1% of Nonidet P-40, and 5 mM $MgCl_2$) supplemented with the cOmplete protease inhibitor cocktail (Roche), phosphatase inhibitor PhosSTOP (Roche), and 500 U of Benzonase for 40 min at 4°C. Lysates were cleared by centrifugation (13,000 × *g*, 4°C, and 5 min). Protein concentration was determined by the Bradford Assay (Bio-Rad). FLAG-tagged ATAD5 proteins were incubated with anti-FLAG M2 agarose affinity beads (Sigma-Aldrich, A2220), and V5-tagged BRD4 proteins were incubated with anti-V5-agarose-affinity beads (Sigma-Aldrich, A7345) for 1 h at 4°C, with constant rotation. The beads were washed three times with buffer X, and the anti-FLAG-bead–bound proteins were eluted with buffer X containing 0.15 mg/ml FLAG peptide. Anti-V5-bead–bound proteins were resuspended in 2 × SDS loading buffer and boiled at 100°C for 5 min. Coimmunoprecipitated proteins were loaded onto SDS-PAGE and analyzed by immunoblotting. The proteins were detected by means of a ChemiDoc MP imaging system (Bio-Rad). The signal intensity of the bands was quantified by ImageLab software version 5.2.1 (Bio-Rad). To detect a phospho-shift, we ran SDS-PAGE in a 5% gel with Phos-Tag™ Acrylamide AAL-107 (25 μM, NARD Institute) and 50 μM $MnCl_2$.

Antibodies

The following antibodies were used: an anti-FLAG antibody (Sigma-Aldrich, F3165, 1:1000); anti-PCNA (PC10) antibody (Santa Cruz Biotechnology, sc-56, 1:2000); Acetyl-Histone H3 Antibody Sampler Kit (Cell Signaling Technology, #9927, 1:2000); Acetyl-Histone H4 Antibody Set (Merck-Millipore, #17-211, 1:2000); anti–histone H3 antibody (Merck-Millipore, #07-690, 1:5000); anti-BRD2 antibody (Bethyl, A302-583A, 1:1000); anti-BRD3 antibody (Bethyl, A302-368A, 1:1000); anti-BRD4 antibody (Bethyl, A301-985A, 1:1000); Pan-BRD4 antibody (Sigma-Aldrich, AV39076, 1:1000); anti-V5 antibody (Sigma-Aldrich, V8137, 1;2000); anti-UAF1 antibody (Santa Cruz Biotechnology, sc-514473, 1:500); anti-S tag antibody (Sigma-Aldrich, SAB2702227, 1:5000); anti-phospho-histone H3 (Ser10) antibody (Cell Signaling Technology, #9706, 1:1000); anti-beta-tubulin antibody (Abcam, ab15568, 1:2000); anti-lamin B1 antibody (Abcam, ab16048, 1:1000); anti-phospho-histone H2A.X (Ser139) (Merck-Millipore, #05-636, 1:2000). The anti-phospho-S653 ATAD5 antibody (1:1000) and anti-human ATAD5 antibody (1:1000) were raised in rabbits.

AP-MS analysis

For liquid chromatography with tandem mass spectrometry, the gel was destained, and bands were cut out and processed as follows. Briefly, the protein bands were divided into 10 mm sections and subjected to in-gel digestion with trypsin. The tryptic digests were separated by online reversed-phase chromatography on a Thermo Scientific Eazy nano LC 1200 UHPLC system equipped with an autosampler using a reversed-phase peptide trap Acclaim PepMap™ 100 column (75 μm inner diameter, 2 cm length) and a reversed-phase PepMap™ RSLC C18 analytical column (75 μm inner diameter, 15 cm length, 3 μm particle size), both from Thermo

Scientific, followed by electrospray ionization at a flow rate of 300 nl/min. The chromatography system was coupled in line with an Orbitrap Fusion Lumos mass spectrometer. Spectra were searched against the UniProt-human DB in Proteome Discoverer 2.1 software via the Sequest-based search algorithm, and comparative analysis of proteins identified in this study was performed in Scaffold 4 Q+S.

CUPID analysis

Plasmids PKC-δ-mRFC-BRD4B and either mNeongreen-ATAD5 (1–692) WT or BET M2 were cotransfected into HEK293T cells. After 48 h, the cells were treated with a translocation signal activator (PMA) and then fixed with 3.7% formaldehyde. CUPID images were captured by means of a laser scanning confocal microscope (LSM 880, Carl Zeiss) with a C-Apochromat 40X/1.2 water immersion lens (488 nm argon laser/505-550 nm detection range for mNeongreen, 561 nm solid state laser/586-662 nm detection range for mRFP). The fluorescence intensity at a cross-section of the nuclear membrane was analyzed in the ZEN blue software (Carl Zeiss).

Protein purification

Proteins for *in vitro* PCNA unloading were purified as described elsewhere (Kang et al., 2019). BRD4A was expressed and purified using a Bac-to-Bac Baculovirus expression system (Thermo Fisher Scientific). The expression construct for BRD4A contains an N-terminal 10 × HIS-tag and a C-terminal 3 × FLAG tag. Viruses were prepared in Sf9 cells, and proteins were expressed in Hi-5 cells. ATAD5 (500–800) and BRD4B (444–794) were cloned into bacterial expression vectors pET-19b (Merck-Millipore) and pRSF-1b (Merck-Millipore), respectively, then were expressed in *E. coli* BL21 (DE3) cells (Enzynomics) and Rosetta 2 (Merck-Millipore). Expression constructs for ATAD5 (500–800) and its BET M2 mutant contain an N-terminal 10 × HIS-3 × FLAG tag and C-terminal StrepII-HALO tag. BRD4B (444–794) was tagged with an N-terminal 6 × HIS-3 × FLAG-MBP tag and C-terminal S tag. To purify proteins from *E. coli* cells, 1 L cultures were grown to OD of 0.4, and protein expression was induced by the addition of 1 M isopropyl β-D-1-thiogalactopyranoside (IPTG) for 4 h incubation. *E. coli* cells were resuspended in Buffer H (25 mM HEPES pH 7.5, 1 mM EDTA, 1 mM EGTA, 2.5 mM magnesium acetate, 10% of glycerol, 1 mM ATP, and 0.02% of NP40) plus 300 mM KCl, with a complete protease inhibitor cocktail (Roche) and were lysed with lysozyme. The cell lysates were cleared by ultracentrifugation (36,000 × *g*, 60 min). Proteins were purified by sequential application of cOmplete HIS-Tag resin (Roche), anti-FLAG M2 agarose resin (Sigma-Aldrich), and ion exchange chromatography. Purified proteins were analyzed by SDS-PAGE.

An *in vitro* pull-down assay

10 pmol of purified wild-type or BET M2 FLAG-ATAD5 (500–800)-StrepII-HALO and 10 pmol of purified MBP-BRD4B (444–794)-S were mixed in Buffer H plus 100 mM KCl for 1 h at 4°C. The mixtures were combined with Streptactin Sepharose beads (GE Healthcare) for 1 h at 4°C. Beads were collected and washed three times with Buffer H plus 100 mM KCl. Bead-associated proteins were eluted with Buffer H plus 100 mM KCl containing 10 mM desthiobiotin, then analyzed by immunoblot or Krypton staining.

Chromatin fractionation

This procedure was performed as described previously (Kang et al., 2019). Cells were lysed with buffer A (100 mM NaCl, 300 mM sucrose, 3 mM $MgCl_2$, 10 mM PIPES pH 6.8, 1 mM EGTA, and 0.2% of Triton X-100, containing the phosphatase inhibitor PhosSTOP (Roche) and cOmplete protease inhibitor cocktail (Roche) for 8 min on ice. Crude lysates were centrifuged at 5000 × *g* at 4°C for 5 min to separate the chromatin-containing pellet from the soluble fraction. The pellet was digested with 50 U of Benzonase (Enzynomics) for 40 min in RIPA buffer (50 mM Tris-HCl pH 8.0, 150 mM NaCl, 5 mM EDTA, 1% of Triton X-100, 0.1% of SDS, 0.5% of sodium deoxycholate, 1 mM PMSF, 5 mM $MgCl_2$, containing the phosphatase inhibitor PhosSTOP (Roche) and cOmplete protease inhibitor cocktail (Roche) to extract chromatin-bound proteins. The chromatin-containing fractions were clarified by centrifugation (13,000 × *g*, 4°C) for 5 min to remove debris. Protein concentration was determined by the Bradford Assay (Bio-Rad), and the proteins were analyzed by western blotting.

The PCNA-unloading reaction

Initially, 20 μL of 2 × loading reaction buffer (50 mM HEPES pH 7.5, 24 mM magnesium acetate, 0.2 mM zinc acetate, 2 mM dithiothreitol, 40 mM phosphocreatine, 12 mM ATP, 0.04% of NP40, 20% of glycerol, 0.8 mg/ml bovine serum albumin, and 2 × cOmplete protease inhibitor cocktail (Roche) was mixed with 20 μL of a protein mixture (25 mM HEPES pH 7.5, 300 mM potassium acetate (KoAc), 1 mM EDTA, 1 mM EGTA, 2.5 mM magnesium acetate, 10% of glycerol, 1 mM dithiothreitol, 1 mM ATP, and 0.02% of NP40) that contains RFC (12.5 nM) and PCNA (250 nM). The PCNA loading reaction was carried out by the addition of 40 μL of the reaction mixture to a bead-conjugated DNA substrate. The reaction mixture was incubated in a Thermomixer (Eppendorf) for 30 min at 37°C and 1200 rpm. After that, the remaining RFC and unbound PCNA were removed by washing the beads once with 0.3 M KCl, twice with 0.5 M KCl, and once again with 0.3 M KoAc Buffer H. For the PCNA-unloading reaction with BRD4, 20 μL of 2 × loading reaction buffer was mixed with 20 μL of the protein mixture that contained various amounts of ATAD5-RLC, with titration by means of various amounts of BRD4. The unloading reaction mixture was added to collect DNA-beads on which PCNA was loaded. The unloading reaction mixture was incubated in a Thermomixer for 15 min at 37°C. Next, the reacted beads were washed with 0.3 M KCl Buffer H three times. Finally, DNA was resuspended in 15 μL of digestion buffer (25 mM Tris-HCl pH 7.5, 100 mM KoAc,

5 mM $CaCl_2$, and 5 mM $MgCl_2$) containing 1 U of DNase I (Promega). DNA was digested for 10 min, beads were separated using a magnet, and the supernatants were collected. PCNA on DNA was quantified by immunoblotting.

An EdU incorporation assay

HeLa cells harboring doxycycline-inducible wild-type or BET M2 ATAD5 (ΔN400) were labeled with 10 μM EdU for 30 min. For flow cytometry, samples were prepared using the Click-iT™ Plus EdU Alexa Fluor™ 647 Flow Cytometry Assay Kit (Invitrogen) and subjected to flow-cytometric analysis (FACSVerse flow cytometer, BD Biosciences). Data were analyzed in the FlowJo software (Tree Star).

QUANTIFICATION AND STATISTICAL ANALYSIS

Quantification of immunoblots was performed using Bio-Rad Image Lab. Statistical analyses were completed using GraphPad Prism. Statistical details of individual experiments are described in the figure legends and results section. Unless otherwise stated, all experiments were performed three times and representative experiments were shown. Bar graphs with mean and standard deviation were presented. Individual data points were overlaid with graphs as scatter dot plot. In all cases, $^{*}p < 0.05$, $^{**}p \leq 0.01$, $^{***}p \leq 0.001$, and $^{****}p \leq 0.0001$.

DATA AND CODE AVAILABILITY

ATAD5 (1-692) interactome data are available via ProteomeXchange with identifier PXD016309. All original data are available upon request.